Accepted Manuscript

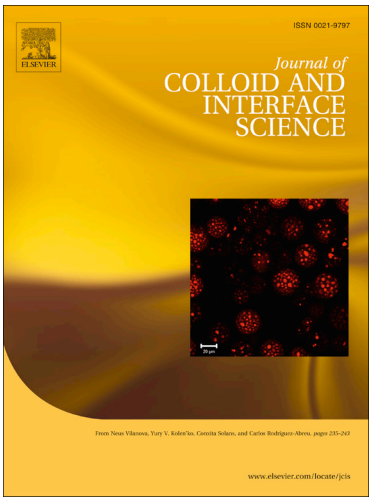

Dual-responsive molybdenum disulfide/copper sulfide-based delivery systems for enhanced chemo-photothermal therapy

Xueyi Zhang, Jianrong Wu, Gareth R. Williams, Yanbo Yang, Shiwei Niu, Qianqian Qian, Li-Min Zhu

PII: S0021-9797(18)31514-5
DOI: https://doi.org/10.1016/j.jcis.2018.12.072
Reference: YJCIS 24449

To appear in: *Journal of Colloid and Interface Science*

Received Date: 22 November 2018
Revised Date: 17 December 2018
Accepted Date: 18 December 2018

Please cite this article as: X. Zhang, J. Wu, G.R. Williams, Y. Yang, S. Niu, Q. Qian, L-M. Zhu, Dual-responsive molybdenum disulfide/copper sulfide-based delivery systems for enhanced chemo-photothermal therapy, *Journal of Colloid and Interface Science* (2018), doi: https://doi.org/10.1016/j.jcis.2018.12.072

Dual-responsive molybdenum disulfide/copper sulfide-based delivery systems for enhanced chemo-photothermal therapy

Xueyi Zhang[a,1], Jianrong Wu[a,1], Gareth R. Williams[b], Yanbo Yang[a], Shiwei Niu[a], Qianqian Qian[a], Li-Min Zhu[a,*]

[a]College of Chemistry, Chemical Engineering and Biotechnology, Donghua University，Shanghai, 201620, China

[b]UCL School of Pharmacy, 29-39 Brunswick Square, London, WC1N 1AX, UK

[1] These authors contributed equally.

* Corresponding author.

Tel: +8621-67792655

E-mail: lzhu@dhu.edu.cn,

Abstract

Molybdenum disulfide (MoS_2)-based drug delivery systems have shown considerable potential in cancer nanomedicines. In this work, a multifunctional nanoplatform comprising MoS_2 nanosheets decorated with copper sulfide (CuS) and further functionalized with polyethylene glycol (PEG) is reported. The resultant material has a particle size of approximately 115 nm, and can be loaded with doxorubicin (DOX) to a loading capacity of 162.3 mg DOX per g of carrier. Drug release is triggered by two stimuli (near infrared (NIR) irradiation and pH), and the carrier is shown to have excellent colloidal stability. The presence of both MoS_2 and CuS leads to very high photothermal conversion efficiency (higher than with MoS_2 alone). *In vitro* experiments revealed that the blank CuS-MoS_2-SH-PEG carrier is biocompatible, but that the synergistic application of chemo-photothermal therapy (in the form of CuS-MoS_2-SH-PEG loaded with DOX and NIR irradiation) led to greater cell death than either chemotherapy (CuS-MoS_2-SH-PEG(DOX) but no NIR) or photothermal therapy (CuS-MoS_2-SH-PEG with NIR). A cellular uptake study demonstrated that the nanoplatform can efficiently enter tumor cells, and that uptake is enhanced when NIR is applied. Overall, the functionalized MoS_2 material developed in this work exhibits great potential as an efficient system for dual responsive drug delivery and synergistic chemo-photothermal therapy. The route employed in our work thus provides a strategy to enhance photothermal efficacy for transition metal dichalcogenide drug delivery systems.

Keywords: MoS_2; drug delivery; chemotherapy; photothermal therapy; synergistic therapy

1. Introduction

Chemotherapy is one of the most commonly used approaches in clinical cancer therapy. It is able to kill metastatic cancer cells efficiently, as well as preventing cell proliferation, but despite this the incidence rate of cancer continues to increase [1]. Furthermore, chemotherapy is not specific to cancer cells, but rather affects all cells simultaneously: this leads to systemic toxicity and damage to healthy tissues. The design of drug delivery systems able to give controlled and targeted release of a chemotherapeutic payload is thus much explored, because they can greatly reduce the side effects of chemotherapy [2].

An alternative to chemotherapy is photothermal therapy (PTT), which is based on the conversion of near infra-red (NIR) light into heat. Absorption of NIR by a photothermal platform located in a tumor can cause thermal ablation, and thus a tumor can be destroyed without recourse to chemical therapies [3-6]. PTT has advantages over chemotherapy in that it provides greater local treatment efficacy, and only minimal systemic side effects. However, there are also disadvantages in terms of the inability of NIR irradiation to penetrate deep into tissues, the risk of inhomogeneous heat distribution, and the possibility that tumor cells will become heat resistant [7-9].

A significant number of nanoscale platforms have been investigated to ameliorate these problems. For instance, much attention has been paid to efficient NIR light absorbing materials such as gold nanostructures, copper chalcogenides, graphene, MoS_2 and carbon nanotubes, among others [10-24]. Researchers have also increasingly begun to recognize the synergistic potential of combining PTT and

chemotherapy in so-called chemo-photothermal therapy. Materials can be designed that both have PTT properties, leading to elevated local temperatures and direct ablation of tumor cells, and where the raised temperature also facilitates drug release from the carrier and enhances uptake by increasing cellular membrane permeability [20, 25]. This offers the possibility of locally delivering a chemotherapeutic to a tumor, massively reducing the systemic side effects. A number of studies have demonstrated that chemo-photothermal therapy has enhanced therapeutic efficiency over either photothermal or chemotherapy alone [26-32].

Stimuli-responsive carriers have the ability to control drug release in response to triggers such as light, magnetic fields, temperature, ultrasound, and pH [33-35]. The blood and tissue of the human body have a roughly neutral pH, while tumors are weakly acidic, and the endosomes in which most materials enter cells have a pH of about 5.0 [36]. These differences can be exploited in pH-targeted drug delivery: for instance, the anti-cancer drug doxorubicin (DOX) is basic, and thus will dissolve more freely at acidic pHs than at neutral pH. A potential carrier for DOX is MoS_2, a layered inorganic solid which responds to NIR irradiation. MoS_2 has been shown to be less toxic than graphene [37], and has been explored as a stimulus-responsive drug carrier in a number of studies [19, 38-40]. There remains room for improvement in its PTT efficacy, however.

To achieve this improvement, the formation of a composite with an additional functional component can be a powerful approach. For MoS_2, copper sulfide (CuS) nanoparticles are suitable in this regard. CuS is low cost and easily synthesized, and

has low cytotoxicity, high stability, and strong NIR absorption [41]. It has been reported that when CuS nanoparticles are grafted on the surface of two-dimensional materials the photothermal conversion efficiency of the nanocomposites improves [42, 43].

In this work, CuS modified MoS_2-nanosheets were prepared, with the aim of developing a dual responsive delivery system for chemo-photothermal therapy (Scheme 1). Further, polyethylene glycol thiol (PEG-SH) was incorporated into the nanocomposites to improve biocompatibility and colloidal stability, and the materials loaded with a doxorubicin (DOX) payload. The materials were fully characterized, and their drug release profiles, *in vitro* cytotoxicity and cellular uptake were explored. The novel drug delivery system produced appears to be a promising therapeutic agent for biomedical applications.

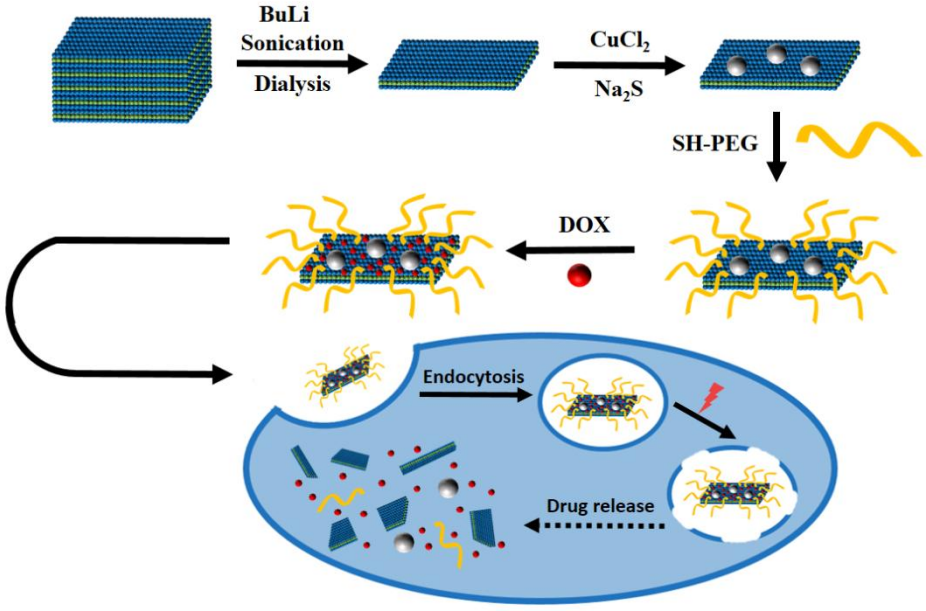

Scheme 1. A schematic illustration of the construction of MoS_2-based nanocomposites for synergistic chemo-photothermal therapy.

2 Materials and methods

2.1 Materials

Doxorubicin (DOX), sodium sulfide (Na_2S), copper (II) chloride ($CuCl_2$) and n-BuLi solution in hexane (2.4 M) were purchased from Aladdin Biochemical Polytron Technologies Inc. Dimethyl sulfoxide (DMSO), fetal bovine serum (FBS), antibiotics (penicillin/streptomycin) and DMEM medium were supplied by the Shanghai Pumai Biotechnology Co., Ltd. 3-(4,5-dimethyl-thiazol-yl)-2,5-diphenyltetrazolium bromide (MTT), MoS_2 powder (2–8 μm, 99%) and phosphate buffered saline (PBS) were purchased from Sigma-Aldrich. 4′-6-diamidino-2-phenylindole (DAPI) was procured from Nanjing Keygen Biotech. MCF-7 cells were purchased from the Type Culture Collection of the Chinese Academy of Sciences. All other materials and dialysis bags were obtained from the Sinopharm Chemical Reagent Co., Ltd. Analytical grade chemicals were used throughout. Milli-Q water with resistance >18.2 MΩ cm was employed for all experiments requiring water.

2.2 Preparation of MoS_2 nanosheets

2 g of MoS_2 was stirred with a solution of n-butyl lithium in hexane (2 mL, 1.6 M) for 48 h under an N_2 atmosphere. After intercalation of lithium was complete, the mixture was washed with hexane to remove residual n-butyl lithium, and the solid product recovered. 30 mL water was added to this product, and the suspension ultrasonicated for 90 min to achieve effective exfoliation. Subsequently, the suspension was centrifuged at 3000 rpm three times to separate the multilayered MoS_2

nanosheets and excess LiOH. The exfoliated MoS_2 was dialyzed against water for 5 days using a cellulose membrane (molecular weight cut-off (MWCO): 10 kDa) to obtain a pure product.

2.3 Preparation of CuS-MoS_2 nanosheets

3 mL of $CuCl_2$ solution (1.60 mg $CuCl_2$, in water) was added to 2 mL of an aqueous suspension containing varied amounts of exfoliated MoS_2 (0.40, 0.80, 1.60, 3.20 or 6.40 mg, in water) and stirred for 2 h. Subsequently, 240 μL of Na_2S solution (50 $\times 10^{-3}$ M, in water) was added to the reaction mixture, with stirring for 5 min. This mixture was transferred to a water bath at 90 °C and stirred for 10 min. The resultant precipitate was dialyzed against water for 3 days using a cellulose membrane (MWCO: 10 kDa) to obtain CuS-MoS_2 nanosheets.

2.4 Functionalization of CuS-MoS_2 nanosheets

SH-PEG (1 mg/mL in water, 5 mL) was added to 2 mL of an aqueous CuS-MoS_2 nanosheet suspension (0.5 mg/mL). After ultrasonication for 30 min, reaction was allowed to proceed for 12 h at room temperature overnight to obtain CuS-MoS_2-SH-PEG. The final product was suspended in water (15 mL) and centrifuged at 8,000 rpm three times to obtain pure CuS-MoS_2-SH-PEG.

2.5 Drug loading

DOX was mixed with CuS-MoS_2-SH-PEG in water and stirred at room temperature overnight. The supernatant was collected by centrifugation and the unloaded DOX concentration determined by UV-vis spectroscopy (UV3600 instrument, Shimadzu Corporation). Experiments were performed with a range of DOX:

CuS-MoS_2-SH-PEG ratios in order to identify the optimum reaction conditions.

2.6 Materials characterization

The morphology of the MoS_2 and CuS-MoS_2 materials was determined using transmission electron microscopy (TEM; JEM-2100 instrument, JEOL). X-ray photoelectron (XPS) spectroscopy (Escalab 250Xi instrument, ThermoFisher) was employed to study the chemical composition of the materials. X-ray diffraction (XRD) measurements were performed on a Bruker D8 Advance X-ray diffractometer supplied with Cu Kα radiation (λ=1.5418 Å). Fourier transform infrared (FT-IR) spectra were recorded on a Nicolet Nexus 870 spectrometer. Zeta potentials were quantified with a ZS90 Zetasizer instrument (Malvern). Dynamic light scattering (DLS) was performed with a Brookhaven BI-200SM instrument. Photothermal effects were analyzed using a laser device (ADR-1860, Shanghai Xilong Optoelectronics Technology Co. Ltd.) at a wavelength of 808 nm.

2.7 *In vitro* drug release

To investigate the NIR and pH responsive release behavior of the formulations, the CuS-MoS_2-SH-PEG nanocomposite was suspended in PBS (0.5 mg/mL, 4 mL, pH 7.4 or pH 5.0) and loaded into a dialysis bag (Mw = 10 kDa). The suspension was dialyzed against different PBS buffers (pH 7.4 or 5.0; 50 mL) with shaking (200 rpm). Additional experiments were performed where the formulation was additionally exposed to 808 nm laser irradiation (1 W/cm^2) for 5 min periodically during the study. The temperature was maintained at 37 °C for all experiments. The concentration of DOX in the release medium was quantified with UV–vis spectroscopy at 480 nm. The

cumulative amount of drug released from the composites was calculated using the formula:

$$\text{Cumulative DOX release } (\%) = \frac{\sum \text{Released DOX}}{\text{Total amount of DOX loaded}} \times 100\%$$

2.8. Photothermal effects

To measure the photothermal conversion efficacy of the CuS-MoS_2-SH-PEG nanocomposites, 1 mL suspensions in PBS (pH 7.4) at concentrations ranging from 0.5 to 2.0 mg/mL were prepared and irradiated with an 808 nm laser (1 W/cm^2). The influence of the laser power density was ascertained by irradiating a 1 mL suspension of CuS-MoS_2-SH-PEG (0.5 mg/mL) under laser power densities from 0.5 to 3 W/cm^2. The thermal stability of the materials was determined by irradiating for 5 min (0.5 W/cm^2) over five on–off cycles. The temperature of the solution was monitored in all cases, using a DT-8891E thermocouple linked to a digital thermometer (Shenzhen Everbest Machinery Industry). The temperature of the solution was assumed to be homogeneous throughout, which is reasonable given the low sample volume of 1 mL. The photothermal conversion efficiency (η) was calculated as follows:

$$\eta = \frac{hS(T_{max}-T_{am})-Q_0}{I(1-10^{-A})}$$

where h is the heat transfer coefficient, S the surface area, T_{max} the equilibrium temperature, T_{am} the ambient temperature, Q_0 the heat absorption of the quartz cell, I the laser power, and A the absorbance of CuS-MoS_2-SH-PEG at 808 nm.

2.9 Cytotoxicity assays

The cytotoxicity of the CuS-MoS_2-SH-PEG nanocomposites on MCF-7 cells was investigated using the MTT assay. MCF-7 cells were grown in DMEM cell culture

medium supplemented with 10% v/v FBS, penicillin (100 U/mL) and streptomycin (100 U/mL). Confluent cells were harvested and plated in 96-well plates at a density of 1 x 10^4 cells per well (200 µL of cell suspension per well). The cells were then co-cultured with CuS-MoS_2-SH-PEG(DOX) or CuS-MoS_2-SH-PEG. Cells were divided into seven treatment groups as follows: 1 PBS; 2 NIR; 3 free DOX; 4 CuS-MoS_2-SH-PEG; 5 CuS-MoS_2-SH-PEG+NIR (photothermal therapy); 6 CuS-MoS_2-SH-PEG(DOX) (chemotherapy); and 7 CuS-MoS_2-SH-PEG(DOX)+NIR (chemo-photothermal therapy). In each group, equivalent DOX concentrations of 0.01 to 10 µg/mL were explored. After incubation for 12 h, the medium was removed and the cells washed with 100 µL PBS, before 100 µL of fresh culture medium was added to the wells. The MCF-7 cells were irradiated with a laser (808 nm, 0.5 W/cm^2) for 5 min in the case of groups 2, 5 and 7.

The MTT reagent (10 µL, 5 mg/mL) was added after 24 hours of culture (5% CO_2, 37 ºC). This was followed by incubation at 37 °C in a 5% CO_2 atmosphere for 4 h. The supernatant was carefully removed, and the MTT-formazan produced by living cells solubilized in 150 µL of DMSO for 20 min. Finally, the absorbance at 490 nm was measured using a microplate reader (MULTSIKAN MK3, ThermoFisher). Cell viability (%) was determined from the absorbance at 450 nm and normalized to negative control wells containing untreated cells.

2.10 *In vitro* cellular uptake

Cell targeting efficiency was investigated with confocal laser scanning microscopy (CLSM). MCF-7 cells were seeded in a 24-well plate (1×10^5 cells per well, 1 mL) and

grown for 24 h. The media was aspirated and 2 mL of fresh DMEM containing free DOX or CuS-MoS_2-SH-PEG(DOX) was added (at a DOX concentration of 3 μg/mL). 3 h later, the cells were rinsed three times with 1 mL of PBS (pH 7.4, 15 min per rinse). Subsequently, the nuclei were stained with DAPI solution and the cells imaged using a Nikon Eclipse Ti-S microscope.

2.11 Statistical analysis

All experiments were repeated three times. The data are displayed as mean ± standard deviation (S.D.). One-way analysis of variance (ANOVA) followed by a post hoc Tukey's test was used for comparison between different groups. Statistical significance was considered at $P < 0.05$ (*), $P < 0.01$ (**) and $P < 0.001$ (***).

3. Results and discussion

3.1 Synthesis and characterization of nanocomposites

The strategy underlying the construction of the CuS-MoS_2-SH-PEG nanocomposites is illustrated in Scheme S1 (Supplementary Information). MoS_2 nanosheets were prepared through a chemical exfoliation protocol, following a previously reported method [26]. Subsequently, CuS nanoparticles were deposited on the surface, giving CuS-MoS_2 [43]. SH-PEG was finally grafted onto the surface of CuS-MoS_2 *via* a thiol reaction. IR spectra (Fig. 1) clearly show the presence of Cu-S stretching modes at 639 cm^{-1} [44] for the samples prepared with all mass ratios of $CuCl_2$ to MoS_2. The successful synthesis of CuS-MoS_2 can thus be confirmed across the range of MoS_2: $CuCl_2$ mass ratios. In the interests of brevity, data will henceforth be shown for CuS-MoS_2-SH-PEG samples prepared with a 2:1 $CuCl_2$: MoS_2 mass ratio, except

where stated otherwise.

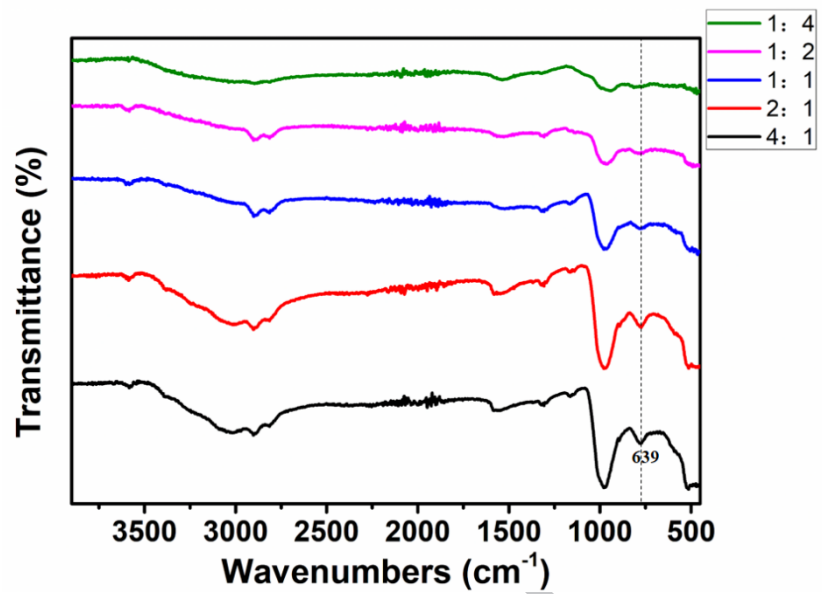

Fig. 1. FT-IR spectra of CuS-MoS_2-SH-PEG synthesized with different mass ratio of CuS to MoS_2 1:4 (green); 1:2 (purple); 1:1 (blue); 2:1 (red); and, 4:1 (black).

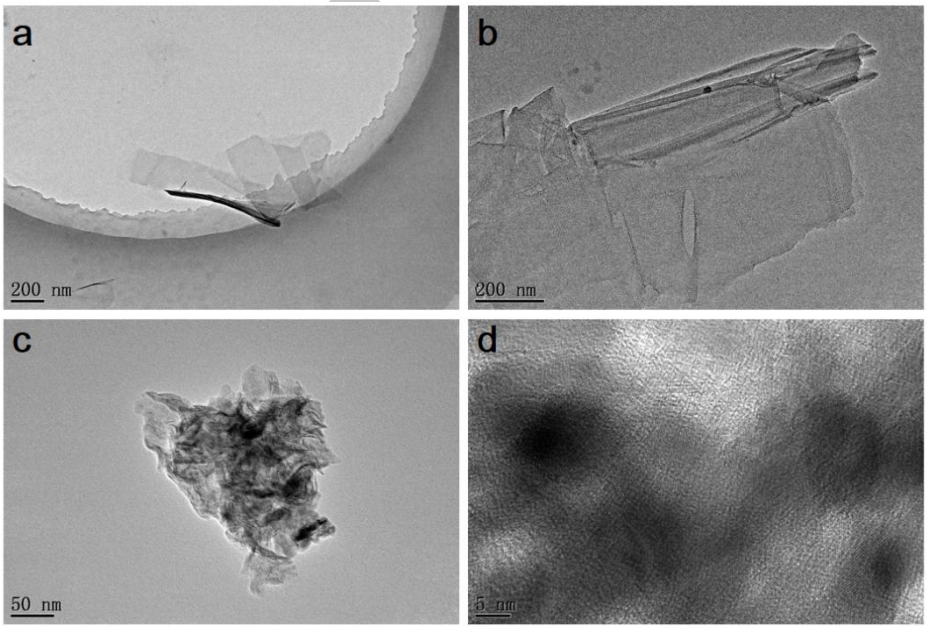

Fig. 2. TEM images of (a, b) the MoS_2 nanosheets and (c, d) CuS-MoS_2.

Fig. 2a and b show TEM images of the exfoliated MoS_2 material. This comprises thin and irregularly shaped sheets, confirming successful exfoliation after BuLi treatment. TEM images of the CuS-MoS_2 material are presented in Fig. 2c and 2d. The surface

of the MoS_2 can be seen to be decorated with numerous CuS NPs.

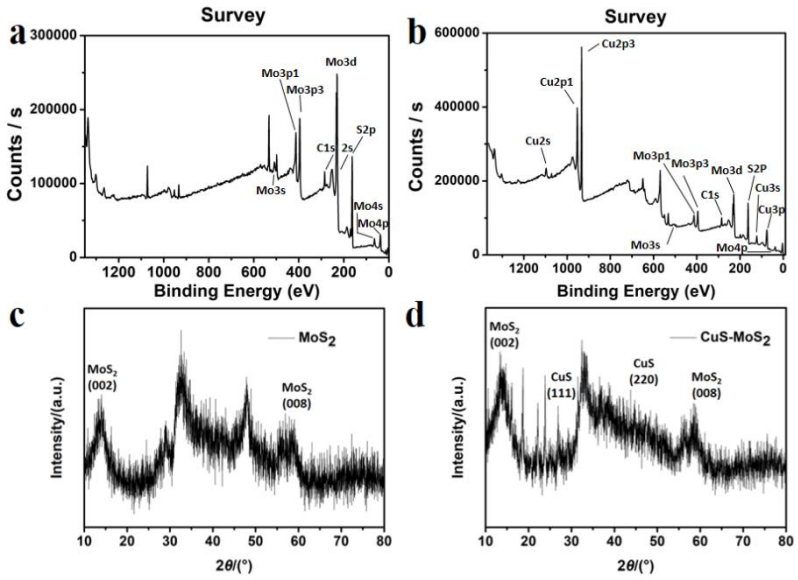

Fig. 3. XPS data for (a) MoS_2 and (b) CuS-MoS_2; XRD diffraction patterns for (c) MoS_2 and (d) CuS-MoS_2.

XPS data for MoS_2 (Fig. 3a) show characteristic peaks of Mo $3p_1$ (413 eV), Mo $3p_3$ (359 eV), Mo 3d (233 eV), and S 2p (175 eV), all of which are consistent with the literature for MoS_2 [45]. The XPS spectrum of CuS-MoS_2 (Fig. 3b) contains additional characteristic peaks associated with Cu 2s (1120 eV), Cu $2p_1$ (953 eV), and Cu $2p_2$ (933 eV). The XRD pattern of MoS_2 (Fig. 3c) matches closely with the literature pattern for MoS_2 (JCPDS10-0319), and that of CuS-MoS_2 (Fig. 3d) contains additional reflections consistent with the presence of CuS (JCPDS 24-0061).

The modification of CuS-MoS_2 by SH-PEG was explored using FTIR spectroscopy. The IR spectra of MoS_2 and CuS-MoS_2-SH-PEG are given in Fig. 4a. A peak at 1640 cm^{-1} in the spectrum of CuS-MoS_2-SH-PEG corresponds to the PEG amide band. A distinct PEG absorption peak at 1100 cm^{-1} can also be clearly seen. These observations verify that CuS-MoS_2-SH-PEG was successfully prepared.

Modification by SH-PEG was further confirmed visually by monitoring the stability of CuS-MoS_2 and CuS-MoS_2-SH-PEG suspensions (see Fig. S1). The colloidal stability of CuS-MoS_2-SH-PEG is much greater than that of CuS-MoS_2: while both formulations are stable after standing for 1 h, after storage for 15 days the latter has sedimented. In contrast, CuS-MoS_2-SH-PEG remains homogeneously dispersed in the carrier medium for at least 15 days, further confirming the coating of SH-PEG.

Zeta potentials were measured to investigate the surface charge of the nanocomposites during the synthesis stages (Fig. 4b). The MoS_2 nanosheets exhibit a zeta potential of -40.6 ± 2.0 mV. The zeta potential of CuS-MoS_2 was -7.3 ± 0.8 mV, and after SH-PEG grafting this changes to -5.3 ± 1.5 mV. The hydrodynamic diameters of the nanocomposites were quantified by DLS, and the data are shown in Fig. 4c. The hydrodynamic diameter of the CuS-MoS_2-SH-PEG nanocomposites is 114.5 nm, which is appropriate for use as a cell-targeted drug delivery system [46].

3.2 *In vitro* drug release

The DOX loading on the nanoparticles was explored as a function of the mass ratio of CuS-MoS_2-SH-PEG to DOX. When the mass ratio was 2:1, 162.3 **±** 9.1 mg DOX could be loaded per g of carrier (Table S1), giving CuS-MoS_2-SH-PEG(DOX). Fig. 4d displays the *in vitro* release behavior of CuS-MoS_2-SH-PEG(DOX) in different pH media (5.0 and 7.4) and with or without laser irradiation (0.5 W/cm^2). It is clear that pH-dependent and NIR-induced DOX release behavior was observed. The release of DOX reached a greater extent at pH 5.0 because of a reduction of the hydrophobic interactions between MoS_2 and DOX and the greater solubility of the latter at low pH

[47]. The release of DOX was faster with laser irradiation than without, which allows release to be triggered by exposure to NIR. Compared to a previous study exploring functionalized MoS_2 delivery systems for DOX, the effect of NIR on DOX release is more apparent here [48]. This can be attributed to the enhanced photothermal efficacy of the CuS modified MoS_2-nanosheets.

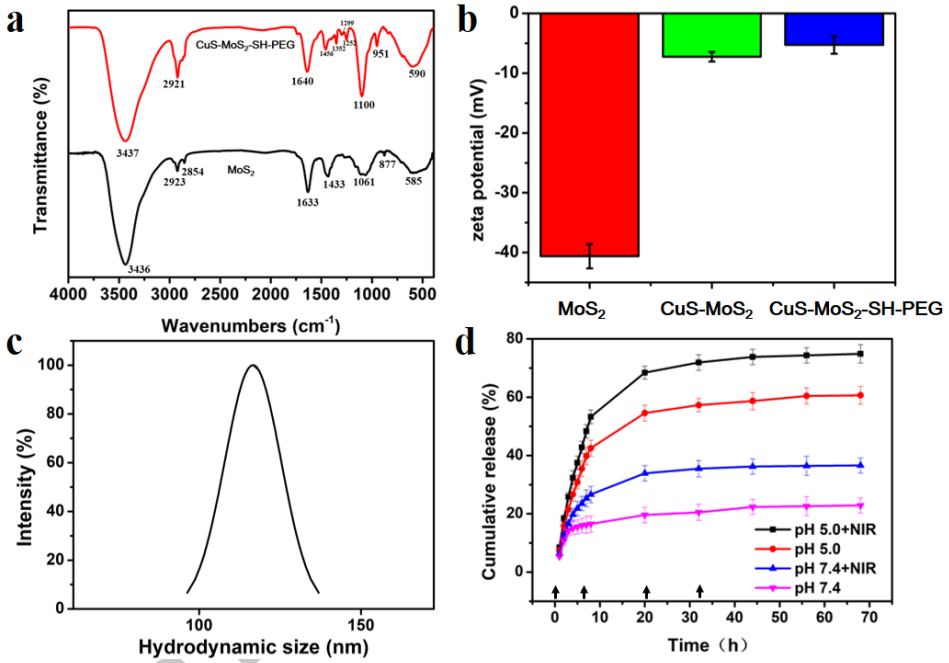

Fig. 4. (a) FT-IR spectra of CuS-MoS_2-SH-PEG (red) and MoS_2 (black); (b) zeta potentials of the nanocomposites at various stages of functionalization; (c) DLS data on CuS-MoS_2-SH-PEG; (d) DOX release profiles for CuS-MoS_2-SH-PEG(DOX) at different pHs, and with or without 808 nm laser irradiation (0.5 W/cm^2). The arrows mark the time points where laser irradiation was applied. Data are presented as mean ± S.D. (n=3).

3.3 Photothermal activity

The use of different mass ratios of $CuCl_2$ to MoS_2 in the preparation of CuS-MoS_2 led to the nanocomposites having varying photothermal conversion efficiency (Fig. 5a). The CuS-MoS_2-SH-PEG system generated with a 1:1 mass ratio of $CuCl_2$ to MoS_2

was used as a baseline, and temperature increases with other mass ratios expressed as a percentage increase on this. At the same laser power and concentration, a $CuCl_2$: MoS_2 ratio of 2:1 leads to the greatest increases in temperature. The photothermal effect of the 2:1 system is found to be concentration-dependent under a fixed irradiation intensity of 0.5 W/cm^2 (Fig. 5b). It also increases with power intensity for a fixed concentration suspension at 0.5mg/mL (Fig. 5c).

The photothermal conversion efficiency of water, CuS-MoS_2-SH-PEG and MoS_2 at the same concentration and laser power density are compared in Fig. 5d. It is clear that CuS-MoS_2-SH-PEG has a better photothermal conversion efficiency than MoS_2. To measure the photothermal stability of CuS-MoS_2-SH-PEG, five on-off cycles of irradiation were carried out (Fig. 5e). The temperature response of the CuS-MoS_2-SH-PEG suspension remains largely constant. The UV–vis absorption spectra of CuS-MoS_2-SH-PEG are also the same before and after five on–off cycles (Fig. 5f). These findings suggest that CuS-MoS_2-SH-PEG has excellent photothermal stability. The photothermal conversion efficiency (Fig. S2) of CuS-MoS_2-SH-PEG was calculated as 59.3%, superior to that reported for another modified MoS_2 system in a previous report [48].

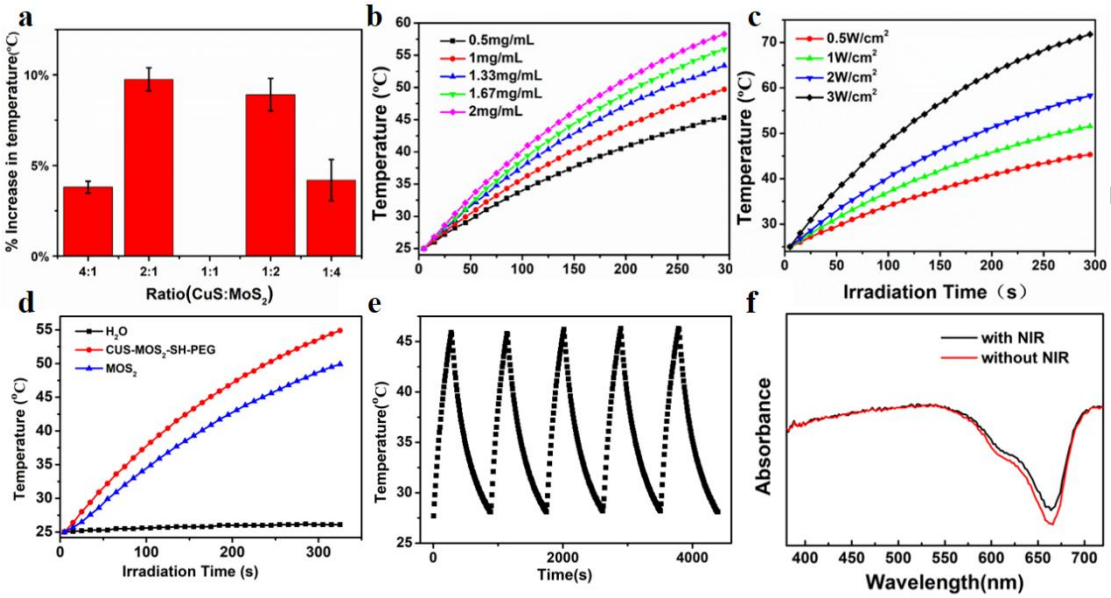

Fig. 5. Photothermal conversion data. (a) Temperature variation of CuS-MoS_2-SH-PEG suspensions (0.5 mg/mL in water, 0.5 W/cm^2) prepared with different mass ratio of CuS and MoS_2. CuS-MoS_2-SH-PEG prepared with 1:1 mass ratio of $CuCl_2$ to MoS_2 was used as a baseline. Data are presented as mean ± SD (n=3); (b) heating curves of CuS-MoS_2-SH-PEG suspensions during exposure to laser power densities of 0.5 W/cm^2; (c) heating curves of CuS-MoS_2-SH-PEG suspensions (0.5 mg/mL) under different laser power densities; (d) heating curves of water, CuS-MoS_2-SH-PEG and MoS_2 at the same concentration under the same laser power density (0.5 mg/mL, 1 W/cm^2); (e) A plot showing the response of CuS-MoS_2-SH-PEG over five on–off cycles (0.5 mg/mL suspension, 0.5 W/cm^2 laser density); (f) UV-vis absorption spectra of CuS-MoS_2-SH-PEG before and after five on–off cycles (0.5 mg/mL suspension, 0.5 W/cm^2 laser density).

3.4 *In vitro* cell viability

The cytocompatibility and therapeutic efficacy of the nanocomposites were evaluated in MCF-7 cells using MTT assays. The cell viabilities of cells treated with either PBS

or NIR and PBS alone were identical (> 90%), indicating that NIR alone has no effect on cell viability (Fig. S3). The results obtained with the other five treatments are shown in Fig. 6. Cells exposed to CuS-MoS_2-SH-PEG alone had high viabilities at 85% or more even with dosing at 10 μg/mL. The carrier thus has good biocompatibility.

The chemotherapeutic effect of CuS-MoS_2-SH-PEG(DOX) was compared to free DOX by treating cells with equivalent doses of the drug. The cell viabilities observed with CuS-MoS_2-SH-PEG(DOX) were lower than cells treated with free DOX at all concentrations, which may be attributed to the low cellular uptake of free DOX. Comparing the cell viabilities of cells treated with CuS-MoS_2-SH-PEG+NIR and CuS-MoS_2-SH-PEG reveals that cell viabilities with the former treatment are lower than the latter, again at all concentrations studied. It is thus clear that the MoS_2 based drug delivery system can exert both chemotherapeutic and PTT effects. Considering the effect of applying both treatments at once, viabilities of cells exposed to CuS-MoS_2-SH-PEG(DOX)+NIR are markedly lower than in the monotherapy groups (chemotherapy or PTT).

The results here thus demonstrate that the MoS_2-based drug delivery system can effectively kill cancerous cells through a synergistic application of both chemotherapy and PTT. The NIR laser irradiation will perform a dual role in this: it both induces heat for photothermal therapy and accelerates the release of DOX from CuS-MoS_2-SH-PEG(DOX) through heat stimulated dissociation of the π–π stacking interactions between CuS-MoS_2-SH-PEG and DOX, which leads to enhanced chemotherapy [49].

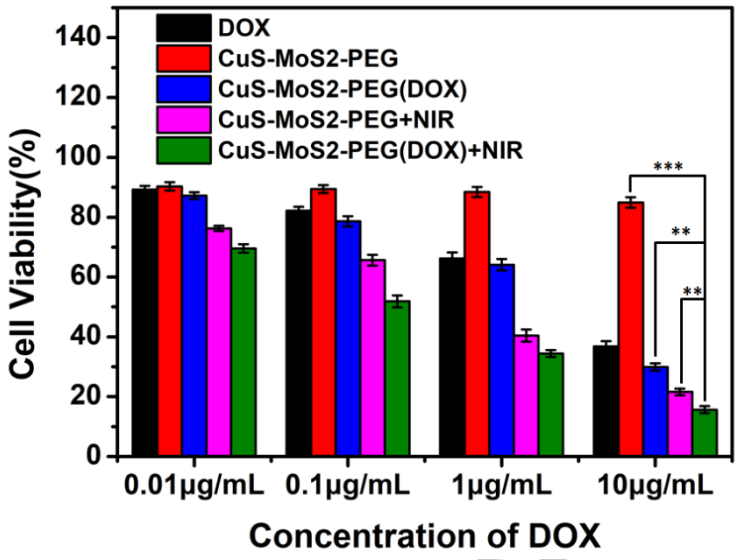

Fig. 6. The viability of MCF-7 cells exposed to different concentrations of DOX or DOX-loaded nanocomposites, with or without laser irradiation.

Statistical significance: $P < 0.01$ (**) and $P < 0.001$ (***). Data are presented as mean ± S.D. (n=3)

3.5 Cellular uptake

The passive targeting ability of the nanocomposites was investigated by CLSM. MCF-7 cells were cultured with free DOX or CuS-MoS_2-SH-PEG(DOX). The MCF-7 cells could take up both free DOX and CuS-MoS_2-SH-PEG(DOX), as shown by the coincident presence of DAPI (blue) and DOX (red) fluorescence (Fig. 7). This effect is minimal in the case of free DOX, but much more noticeable when the DOX is loaded on the nanocarrier. There is hence greater cellular uptake of CuS-MoS_2-SH-PEG(DOX) by MCF-7 cells than of free DOX. MCF-7 cells incubated with CuS-MoS_2-SH-PEG (DOX)+NIR exhibited still greater DOX fluorescence than those exposed to CuS-MoS_2-SH-PEG(DOX). This can be attributed to the NIR light

enhancing the cellular uptake of CuS-MoS_2-SH-PEG(DOX) mainly because the mild local hyperthermia induced will cause minor disruptions to the cell membrane, rendering it more permeable [50, 51]. Overall, these results suggest that the CuS-MoS_2-SH-PEG(DOX) formulation can efficiently deliver DOX into MCF-7 cells, which is beneficial for combined chemo-photothermal therapy. However, it should be noted that less DOX fluorescence was observed here compared to other MoS_2-based systems conjugated with ligands for receptor-mediated uptake and active targeting [26, 48]. This confirms the benefits of using targeting ligands to enhance cellular uptake.

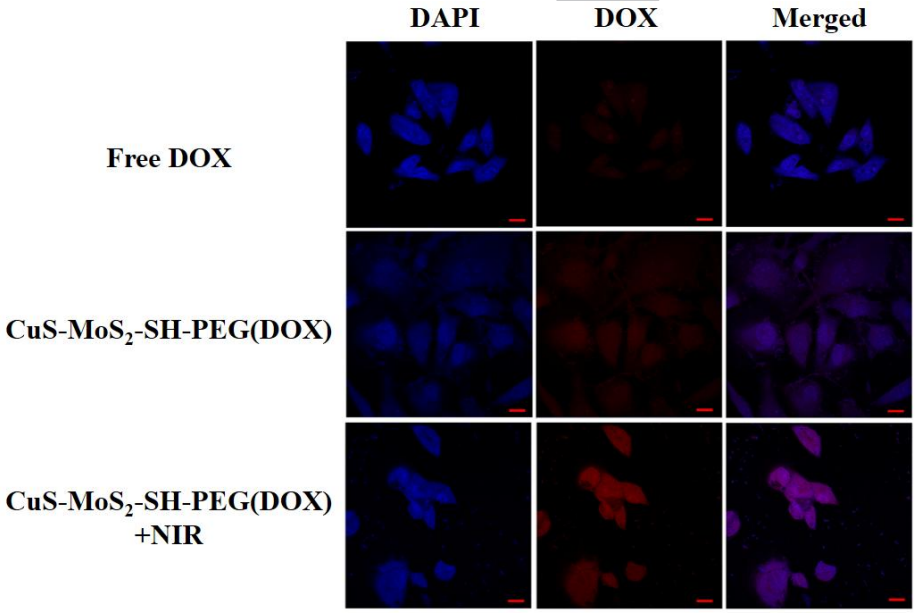

Fig. 7. Confocal microscope images of MCF-7 cells incubated with CuS-MoS_2-SH-PEG, DOX or CuS-MoS_2-SH-PEG(DOX) at an equivalent DOX concentration of 5.0 μg/mL for 4 h. Scale bar: 25μm

4. Conclusions

In this work, a multifunctional drug delivery system for combined photothermal and chemotherapy was prepared. This comprises molybdenum disulfide nanosheets surface modified with copper sulfide and further functionalized with polyethylene

glycol thiol (PEG-SH). The successful generation of the nanocomposite was verified with electron microscopy, X-ray diffraction, X-ray photoelectron spectroscopy, and FT-IR spectroscopy. The CuS-MoS_2-SH-PEG particles were ca. 115 nm in size, and form a colloidal aqueous suspension which is stable for at least 15 days. The nanocomposites have a high drug loading capacity of 162.3 mg doxorubicin (DOX)/g CuS-MoS_2-SH-PEG. The nanoplatform shows potent photothermal effects upon irradiation with near infrared (NIR) irradiation, with the CuS modification leading to a clear improvement in this regard. The greatest photothermal efficacy is found with materials prepared with a 2:1 $CuCl_2$: MoS_2 mass ratio. CuS-MoS_2-SH-PEG(DOX) displays pH-responsive and NIR induced drug release behavior, which is promising for tumor-specific delivery. *In vitro* studies found that the cytotoxicity of the CuS-MoS_2-SH-PEG(DOX) formulation is greatest when NIR irradiation is applied, and the application of combined chemo-photothermal therapy led to greater cell death than either monotherapy alone (chemotherapy or photothermal therapy [PTT]). The cellular uptake of CuS-MoS_2-SH-PEG(DOX) by cancer cells was much greater than that of free DOX, and was enhanced by NIR exposure. Overall, our study suggests that the CuS-MoS_2-SH-PEG nanoparticles may be a promising platform for advanced anti-cancer therapeutics, and offers significantly enhanced PTT efficacy over previous reports of functionalized MoS_2 systems [48]. Our approach provides a strategy to enhance photothermal efficacy for a range of transition metal dichalcogenide drug delivery systems.

Acknowledgements

This research was financially supported by the Shanghai Municipal Science and Technology Commission Project 16410723700, the Biomedical Textile Materials "111 Project" of the China Ministry of Education (No B07024) and the UK-China Joint Laboratory for Therapeutic Textiles (based at Donghua University).

References

[1] F. Fu, Y. Wu, J. Zhu, S. Wen, M. Shen, X. Shi, Multifunctional Lactobionic Acid-Modified Dendrimers for Targeted Drug Delivery to Liver Cancer Cells: Investigating the Role Played by PEG Spacer, ACS Appl. Mater. Inter. 6 (2014) 16416-16425.

[2] T. Shao, J. Wen, Q. Zhang, Y. Zhou, L. Liu, L. Yuwen, Y. Tian, Y. Zhang, W. Tian, Y. Su, NIR Photoresponsive Drug Delivery and Synergistic Chemo-Photothermal Therapy by Monodispersed MoS_2 Nanosheets Wrapped Periodic Mesoporous Organosilicas, J. Mater. Chem. B. 4 (2016) 7708-7717.

[3] W. Chen, K. Zeng, H. Liu, J. Ouyang, L. Wang, Y. Liu, H. Wang, L. Deng, Y.N. Liu, Cell Membrane Camouflaged Hollow Prussian Blue Nanoparticles for Synergistic Photothermal - hChemotherapy of Cancer, Adv. Funct. Mater.27 (2017) 1605795.

[4] B. Xia, B. Wang, J. Shi, Y. Zhang, Q. Zhang, Z. Chen, J. Li, Photothermal and biodegradable polyaniline/porous silicon hybrid nanocomposites as drug carriers for combined chemo-photothermal therapy of cancer, Acta. Biomater. 51 (2017) 197-208.

[5] X. Li, L. Xing, Y. Hu, Z. Xiong, R. Wang, X. Xu, L. Du, M. Shen, X. Shi, An RGD-modified hollow silica@Au core/shell nanoplatform for tumor combination therapy, Acta. Biomater. 62

(2017) 273-283.

[6] X. Li, L. Xing, K. Zheng, P. Wei, L. Du, M. Shen, X. Shi, Formation of Gold Nanostar-Coated Hollow Mesoporous Silica for Tumor Multimodality Imaging and Photothermal Therapy, ACS Appl. Mater. Inter9 (2017) 5817-5827.

[7] T. Bao, W. Yin, X. Zheng, X. Zhang, J. Yu, X. Dong, Y. Yong, F. Gao, L. Yan, Z. Gu, One-pot synthesis of PEGylated plasmonic MoO(3-x) hollow nanospheres for photoacoustic imaging guided chemo-photothermal combinational therapy of cancer, Biomaterials 76 (2016) 11-24.

[8] J. Chen, X. Li, X. Liu, H. Yan, Z. Xie, Z. Sheng, X. Gong, L. Wang, X. Liu, P. Zhang, Hybrid $MoSe_2$-indocyanine green nanosheets as a highly efficient phototheranostic agent for photoacoustic imaging guided photothermal cancer therapy, Biomater. Sci. 6 (2018) 1503-1516.

[9] K. Wang, Y. Zhang, J. Wang, A. Yuan, M. Sun, J. Wu, Y. Hu, Self-assembled IR780-loaded transferrin nanoparticles as an imaging, targeting and PDT/PTT agent for cancer therapy, Sci. Rep. 6 (2016) 27421.

[10] L. Zhang, Z. Yang, W. Zhu, Z. Ye, Y. Yu, Z. Xu, J. Ren, P. Li, Dual-stimuli Responsive Polymer Microspheres Encapsulated CuS Nanoparticles for Magnetic Resonance Imaging-Guided Synergistic Chemo-Photothermal Therapy, ACS Biomater. Sci. Eng. 3 (2017) 1690-1701.

[11] M. Zhou, J. Li, S. Liang, A.K. Sood, D. Liang, C. Li, CuS Nanodots with Ultrahigh Efficient Renal Clearance for Positron Emission Tomography Imaging and Image-Guided Photothermal Therapy, Acs Nano, 9 (2015) 7085-7096.

[12] Y.W. Chen, Y.L. Su, S.H. Hu, S.Y. Chen, Functionalized graphene nanocomposites for enhancing photothermal therapy in tumor treatment, Adv. Drug. Deliver. Rev. 105 (2016) 190-204.

[13] B. Du, C. Ma, G. Ding, H. Xu, L. Dan, E. Wang, W. Jin, Cooperative Strategies for

Enhancing Performance of Photothermal Therapy (PTT) Agent: Optimizing Its Photothermal Conversion and Cell Internalization Ability, Small 13 (2017) 1603275.

[14] A.J. Trinidad, S.J. Hong, Q. Peng, S.J. Madsen, H. Hirschberg, Combined concurrent photodynamic and gold nanoshell loaded macrophage-mediated photothermal therapies: an in vitro study on squamous cell head and neck carcinoma, Laser Surg Med. 46 (2014) 310-318.

[15] J.T. Robinson, S.M. Tabakman, Y. Liang, H. Wang, H.S. Casalongue, D. Vinh, H. Dai, Ultrasmall reduced graphene oxide with high near-infrared absorbance for photothermal therapy, J. Am. Chem. Soc. 133 (2011) 6825-6831.

[16] W. Zhang, Z. Guo, D. Huang, Z. Liu, X. Guo, H. Zhong, Synergistic effect of chemo-photothermal therapy using PEGylated graphene oxide, Biomaterials 32 (2011) 8555-8561.

[17] K. Yang, L. Hu, X. Ma, S. Ye, L. Cheng, X. Shi, C. Li, Y. Li, Z. Liu, Multimodal imaging guided photothermal therapy using functionalized graphene nanosheets anchored with magnetic nanoparticles, Adv. Mater. 24 (2012) 1868-1872.

[18] S.S. Chou, B. Kaehr, J. Kim, B.M. Foley, M. De, P.E. Hopkins, J. Huang, C.J. Brinker, V.P. Dravid, Chemically Exfoliated MoS_2 as Near-Infrared Photothermal Agents, Angew. Chem., Int. Ed. 125 (2013) 4254-4258.

[19] T. Liu, C. Wang, X. Gu, H. Gong, L. Cheng, X. Shi, L. Feng, B. Sun, Z. Liu, Drug Delivery with PEGylated MoS2 Nano-sheets for Combined Photothermal and Chemotherapy of Cancer, Adv. Mater. 26 (2014) 3433-3440.

[20] T. Liu, C. Wang, W. Cui, H. Gong, C. Liang, X. Shi, Z. Li, B. Sun, Z. Liu, Combined photothermal and photodynamic therapy delivered by PEGylated MoS2 nanosheets, Nanoscale6 (2014) 11219-11225.

[21] L. Hou, X. Yang, J. Ren, Y. Wang, H. Zhang, Q. Feng, Y. Shi, X. Shan, Y. Yuan, Z. Zhang, A novel redox-sensitive system based on single-walled carbon nanotubes for chemo-photothermal therapy and magnetic resonance imaging, Int. J. Nanomed. 11 (2016) 607.

[22] J. Song, W. Feng, X. Yang, N. Bo, M.G. Harp, S.H. Culp, H. Song, H. Peng, L. Nie, J. Chen, Gold Nanoparticle Coated Carbon Nanotube Ring with Enhanced Raman Scattering and Photothermal Conversion Property for Theranostic Applications, J. Am. Chem. Soc. 138 (2016) 7005-7015.

[23] C. Yan, Q. Tian, S. Yang, Recent advances in the rational design of copper chalcogenide to enhance the photothermal conversion efficiency for the photothermal ablation of cancer cells, RSC. Adv. 7 (2017) 37887-37897.

[24] Y. Yong, X. Cheng, T. Bao, M. Zu, L. Yan, W. Yin, C. Ge, D. Wang, Z. Gu, Y. Zhao, Tungsten Sulfide Quantum Dots as Multifunctional Nanotheranostics for In Vivo Dual-Modal Image-Guided Photothermal/Radiotherapy Synergistic Therapy, ACS Nano 9 (2015) 12451-12463.

[25] K. Dong, Z. Liu, Z. Li, J. Ren, X. Qu, Hydrophobic anticancer drug delivery by a 980 nm laser-driven photothermal vehicle for efficient synergistic therapy of cancer cells in vivo, Adv. Mater. 25 (2013) 4452-4458.

[26] J. Wu, D.H. Bremner, S. Niu, H. Wu, J. Wu, H. Wang, H. Li, L.M. Zhu, Functionalized MoS_2 nanosheet-capped periodic mesoporous organosilicas as a multifunctional platform for synergistic targeted chemo-photothermal therapy, Chem. Eng. J. 342 (2018) 90-102.

[27] W. Yin, L. Yan, J. Yu, G. Tian, L. Zhou, X. Zheng, X. Zhang, Y. Yong, J. Li, Z. Gu, High-Throughput Synthesis of Single-Layer MoS_2 Nanosheets as a Near-Infrared

Photothermal-Triggered Drug Delivery for Effective Cancer Therapy, ACS Nano. 8. (2014) 6922-6933.

[28] R.K. Thapa, S.Y. Yu, J.H. Jeong, H.G. Choi, C.S. Yong, J.O. Kim, Graphene oxide-wrapped PEGylated liquid crystalline nanoparticles for effective chemo-photothermal therapy of metastatic prostate cancer cells, Colloid. Surface. B.143 (2016) 271-277.

[29] Y.S. Yun, Z. Teng, Y. Hui, J.W. Shou, T. Ying, L.Z. Yun, F.L. Wen, T. Wei, J.Z. Li, L. Nan, A Multifunctional PB@mSiO_2-PEG/DOX Nanoplatform for Combined Photothermal-Chemotherapy of Tumor, ACS Appl. Mater. Inter. 8 (2016) 17038-17046.

[30] M. Ma, H. Chen, Y. Chen, X. Wang, F. Chen, X. Cui, J. Shi, Au capped magnetic core/mesoporous silica shell nanoparticles for combined photothermo-/chemo-therapy and multimodal imaging, Biomaterials 33 (2012) 989-998.

[31] X. Wang, J. Zhang, Y. Wang, C. Wang, J. Xiao, Z. Qiang, Y. Cheng, Multi-responsive photothermal-chemotherapy with drug-loaded melanin-like nanoparticles for synergetic tumor ablation, Biomaterials 81 (2016) 114-124.

[32] S. Duan, Y. Yang, C. Zhang, N. Zhao, F.J. Xu, NIR-Responsive Polycationic Gatekeeper-Cloaked Hetero-Nanoparticles for Multimodal Imaging-Guided Triple-Combination Therapy of Cancer, Small, 13 (2016) 1603133.

[33] Z. Deng, Z. Zhen, X. Hu, S. Wu, Z. Xu, P.K. Chu, Hollow chitosan–silica nanospheres as pH-sensitive targeted delivery carriers in breast cancer therapy, Biomaterials,32 (2011) 4976-4986.

[34] V. Shanmugam, S. Selvakumar, C.S. Yeh, ChemInform Abstract: Near-Infrared Light-Responsive Nanomaterials in Cancer Therapeutics, Chem. Soc. Rev., 45 (2015) 6254-6287.

[35] K.J. Chen, H.F. Liang, H.L. Chen, Y. Wang, P.Y. Cheng, H.L. Liu, Y. Xia, H.W. Sung, A Thermoresponsive Bubble-Generating Liposomal System for Triggering Localized Extracellular Drug Delivery, ACS Nano 7 (2013) 438-446.

[36] K. Sakai-Kato, N. Nishiyama, M. Kozaki, T. Nakanishi, Y. Matsuda, M. Hirano, H. Hanada, S. Hisada, H. Onodera, H. Harashima, General considerations regarding the in vitro and in vivo properties of block copolymer micelle products and their evaluation, J. Control. Release. 210 (2015) 76-83.

[37] W.Z. Teo, E.L. Chng, Z. Sofer, M. Pumera, Cytotoxicity of exfoliated transition-metal dichalcogenides (MoS_2 , WS_2 , and WSe_2) is lower than that of graphene and its analogues, Chem.Eur. J. 20 (2014) 9627-9632.

[38] S. Wang, Y. Chen, X. Li, W. Gao, L. Zhang, J. Liu, Y. Zheng, H. Chen, J. Shi, Injectable 2D MoS_2-Integrated Drug Delivering Implant for Highly Efficient NIR-Triggered Synergistic Tumor Hyperthermia, Adv. Mater. 27 (2015) 7117-7122.

[39] X. Dong, W. Yin, X. Zhang, S. Zhu, X. He, J. Yu, J. Xie, Z. Guo, L. Yan, X. Liu, Intelligent MoS_2 Nanotheranostic for Targeted and Enzyme/pH/NIR-Responsive Drug Delivery to Overcome Cancer Chemotherapy Resistance Guided by PET Imaging, ACS Appl. Mater. Inter. 10 (2018) 4271-4284.

[40] C.H. Park, S. Lee, G. Pornnoppadol, Y.S. Nam, S.H. Kim, B.J. Kim, Microcapsules Containing pH-Responsive, Fluorescent Polymer-Integrated MoS_2: Effective Platform for in-situ pH Sensing and Photothermal Heating, ACS Appl. Mater. Inter. 10 (2018) 9023-9031.

[41] M. Zhou, R. Zhang, M. Huang, W. Lu, S. Song, M.P. Melancon, M. Tian, D. Liang, C. Li, A chelator-free multifunctional [64Cu]CuS nanoparticle platform for simultaneous micro-PET/CT

imaging and photothermal ablation therapy, J. Am. Chem. Soc. 132 (2010) 15351-15358.

[42] J. Bai, Y. Liu, X. Jiang, Multifunctional PEG-GO/CuS nanocomposites for near-infrared chemo-photothermal therapy, Biomaterials. 35 (2014) 5805-5813.

[43] X. Meng, Z. Liu, Y. Cao, W. Dai, K. Zhang, H. Dong, X. Feng, X. Zhang, Fabricating Aptamer-Conjugated PEGylated-MoS2/Cu1.8S Theranostic Nanoplatform for Multiplexed Imaging Diagnosis and Chemo-Photothermal Therapy of Cancer, Adv. Funct. Mater. 27 (2017) 1605592.

[44] J. Balavijayalakshmi, S. Manju, Investigation of structural, optical and morphological properties of copper doped zinc sulphide nanoparticles, Mat. Sci. Semicon. Proc. 48 (2016) 101-105.

[45] X. Yang, W. Fu, W. Liu, J. Hong, Y. Cai, C. Jin, M. Xu, H. Wang, D. Yang, H. Chen, Engineering crystalline structures of two-dimensional MoS_2 sheets for high-performance organic solar cells, J. Mater. Chem. A, 2.(2014) 7727-7733.

[46] D.R. Elias, A. Poloukhtine, V. Popik, A. Tsourkas, Effect of ligand density, receptor density, and nanoparticle size on cell targeting, Nanomed. Nanotechnol. 9 (2013) 194-201.

[47] J. Zhu, L. Liao, X. Bian, J. Kong, P. Yang, B. Liu, pH-controlled delivery of doxorubicin to cancer cells, based on small mesoporous carbon nanospheres, Small 8 (2012) 2715-2720.

[48] X. Zhang, J. Wu, G.R. Williams, S. Niu, Q. Qian, L.-M. Zhu, Functionalized MoS_2-nanosheets for targeted drug delivery and chemo-photothermal therapy, Colloids and surfaces. B, Biointerfaces. 173 (2018) 101-108.[49] A. Topete, M. Alatorremeda, P. Iglesias, E.M. Villaralvarez, S. Barbosa, J.A. Costoya, P. Taboada, V. Mosquera, Fluorescent Drug-Loaded, Polymeric-Based, Branched Gold Nanoshells for Localized Multimodal Therapy and Imaging of

Tumoral Cells, ACS Nano, 8 (2014) 2725-2738.

[50] Y. Sun, T. Shi, L. Zhou, Y. Zhou, B. Sun, X. Liu, Folate-decorated and NIR-activated nanoparticles based on platinum(IV) prodrugs for targeted therapy of ovarian cancer, J Microencapsul, 34 (2017) 675-686.[51] N. Lu, P. Huang, W. Fan, Z. Wang, Y. Liu, S. Wang, G. Zhang, J. Hu, W. Liu, G. Niu, R.D. Leapman, G. Lu, X. Chen, Tri-stimuli-responsive biodegradable theranostics for mild hyperthermia enhanced chemotherapy, Biomaterials,126 (2017) 39-48.

Graphical abstract